Understanding particle deposition kinetics on NF membranes

Understanding particle deposition kinetics on NF membranes: a focus on micro-beads & membrane interactions at different environmental conditions

Huayu Cao[a], Olivier Habimana[a], Andrea J.C. Semião[b], Ashley Allen[a], Rory Heffernan[a], Eoin Casey[a *]

[a]School of Chemical and Bioprocess Engineering, University College Dublin (UCD), Belfield,

Dublin 4, IRELAND

[b] School of Engineering, University of Edinburgh, UK EH9 3JL

* Corresponding author: Email: eoin.casey@ucd.ie ; Tel: +353 (0) 1 716 1877

ABSTRACT

The significance of nanofiltration membrane surface properties when interacting with microbeads with and without permeate flux was investigated. This was achieved by characterising the surface tension and zeta potential of micro beads and NF90 membranes to determine the colloid-membrane interaction forces. Dynamic adhesion assays under different ionic strengths (0.1M and 0.01M) and pH (5, 7, 9) were conducted. Experimental results showed that at high ionic strength, pH does not have a significant effect on adhesion rates, while at low ionic strength the adhesion rate increased at pH 7 (4.56 s^{-1} cm^{-2}) compared to pH 5 and pH 9, with rates of 2.69 and 3.66 s^{-1} cm^{-2} respectively. A model was devised to predict colloidal adhesion onto membranes under increasing permeate flux conditions, taking into account all interaction forces. Model predictions indicate that drag force overwhelms all other colloid-membrane interaction forces when the permeate flux increases to 7.2 L hr^{-1} m^{-2} . This study suggests that altering membrane surface properties for the prevention of fouling may be limited in its success as an antifouling strategy.

KEYWORDS

adhesion; nanofiltration; XDVLO; biofouling; microbead

Graphical Abstract

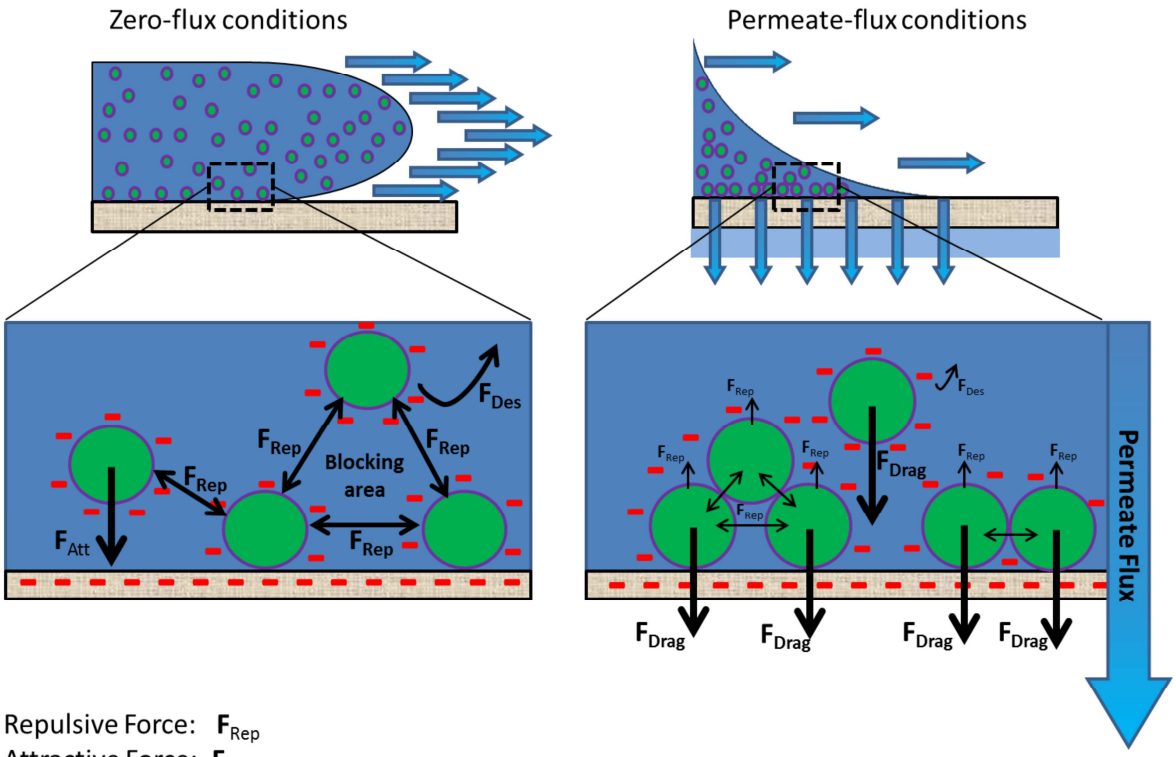

Repulsive Force: F_{Rep}
Attractive Force: F_{Att}
Desorption Force: F_{Des}
Drag Force: F_{Drag}

INTRODUCTION

Biofouling has been recognised as one of the main impediments to performance of membrane processes such as reverse osmosis (RO) and nanofiltration (NF) applied to water treatment[1], in the form of increased hydraulic resistance, decreased permeability or lower salt rejection [2-4]. Biofouling is initiated by the adhesion of microorganisms onto surfaces [5] and consequently an understanding of the mechanisms involved during initial adhesion is an important aspect of the development of a full understanding biofilm development. In particular, there is need for a better understanding of the interactions between suspended bacterial cells and NF membrane surfaces. Key parameters include the effects of hydrodynamics and its effect on mass transfer rate, the surface properties of the membrane and bacteria, liquid solution properties such as pH and ionic strength, as well as permeate drag exerted on bacteria [6-12].

It is acknowledged that hydrodynamics affect the mass transfer rate of bacteria to the surface by the process of convection diffusion. In an earlier study in which bacterial adhesion under dynamic conditions was investigated onto different surfaces, Meinders and colleagues demonstrated that it was possible to study mass transfer processes precisely under constant flow experimental conditions[10]. The effect of mass transfer on bacterial adhesion can generally be described by the adsorption-desorption kinetic model. The potential adhesion area is blocked by the previous adhered microorganisms and this blocking effect leads to the equilibrium status [10, 13]. Bacterial adhesion onto membranes was also shown to be associated with to the surface physicochemical properties of both bacteria and substrate. Subramani and Hoek reported that hydrophobic RO/NF polyamide membranes rather than hydrophilic membranes favoured bacterial adhesion [8]. Miller et al found similar results that hydrophilized polysulfone ultrafiltration membaranes(modified by Polydopamine and polydopamine-*g*-poly ethylene glycol)showed significantly reduced adhesion of bovine serum albumin and *P. aeruginosa* during one hour static adhesion tests. [12] Moreover, the

growth phase of bacterial cells was also shown to influence cell-wall properties; Sharon and colleagues observed that stationary phase *Escherichia coli* cells were more adhesive than those in mid-exponential phase, generated by distinct heterogeneities in local charge sites of the cell's outer-membrane during stationary phase[14]. The environmental conditions are also known to affect adhesion behaviour; Subramani and Hoek demonstrated that high ionic strength environments led to higher rates of bacterial adhesion as a result of compressed double layer repulsion between the bacteria and substratum[8]. Permeate flux is also considered to be an important factor affecting initial bacterial adhesion onto membranes. Subramani and Hoek also reported that permeation drag dominated the initial deposition of cells onto NF90 membranes at ionic strength environments of 0.01M and at flux conditions larger than 20L hr^{-1} m^{-2} [8]. However, to our knowledge, there are no published studies describing a mathematical model capable of predicting bacterial surface coverage under permeate flux conditions, taking into account the adsorption-desorption kinetic model based on particle blocking effects and the XDLVO theory.

To successfully implement such a model, there are several aspects of bacterial adhesion modelling that still need to be developed. According to Meinders et al , adsorption and desorption rates were determined from the image subtraction technique with images taken at the centre of the bottom plate every 12 s [10]. However, focusing on one point makes it difficult to characterise adhesion over a larger scale or area , as was the case in a study presented by Bos et al(1999), in which the Sherwood number was shown to be related to the longitudinal distance to the inlet[9]. To address this limitation, Sjollema and Busscher (1990) developed an image analysis technique using a radial distribution function to determine the blocking effect between deposited particles on the substrum surfaces when the steady state of bead adhesion is reached [13]. Furthermore a comprehensive statistical analysis can be achieved by combining random image acquisition with radial distribution analysis.

There are several challenges to modelling bacterial surface interactions due in part to the complex and heterogeneous nature of the cell outer-membrane [15]. In an effort to better eliminate these effects and to validate mathematical models it is sometimes useful to employ abiotic particles that have similarities to bacteria [10, 13]. Brant and Childress used alumina, silica and polystyrene colloids to assess short range interactions between the particle and membrane. The XDLVO approach was successfully used to predict the occurrence of fouling of three different colloids on the FT-30 membrane[16]. Meinders et al used polystyrene beads as model foulants and compared the bead adhesion with bacterial adhesion on glass and PMMA (polymethylmethacrylate) [10]. It was observed that the polystyrene beads had a lower deposition efficiency (0.1) than *Streptococcus thermophilus* B(1.8). This is due to the attractive force of the beads (-5×10^{-12}N) being weaker than that of the bacteria (-15×10^{-12}N).

The objectives of this study were firstly to experimentally determine the deposition kinetics of micro beads using the parallel plate flow cell, secondly to correlate the interaction energies between the colloid and the surface with a kinetic model and to use the model to gain an understanding of the impact of pH, ionic strength and surface energy on the transport of micro beads to glass or membrane surfaces; and thirdly to predict the surface coverage of micro beads or bacteria on nanofiltration membranes with the presence of permeate flux using the kinetic parameters and XDLVO force calculated from the model.

MATERIALS AND METHODS

Micro bead preparation and characterization.

Green fluorescent carboxylate micro beads (Sigma, L4530) of 2 μm diameter were used for all adhesion experiments. A concentrated micro bead solution was first diluted (1:30) in Grade 1 pure water (18.2 MΩ cm^{-1}) obtained from an Elga Process Water System (Biopure 15 and Purelab flex 2,

Veolia, Ireland), hereafter referred to as MilliQ water. The suspension was then centrifuged at 10,000 RPM for 10 minutes. The supernatant was carefully discarded and the micro bead re-suspended with 25 µl volume of MilliQ . This sequence was repeated three times to remove any trace of surfactants from the solution the micro beads were provided in.

Prior to characterization and adhesion experiments, micro bead pellets were re-suspended in their respective reconstructed PBS-buffer at selected pH conditions. The PBS buffer solutions comprised Sodium phosphate monobasic (Sigma, Ireland) and Sodium phosphate dibasic (Sigma, Ireland) to 0.1 M and 0.01 M ionic strengths. The pH of each buffer solution was adjusted with 0.01 M sodium hydroxide (NaOH, analytical grade, Sigma Ireland) or phosphoric acid solution (H_3PO_4, analytical grade, Sigma,Ireland) to pH values of 5, 7 or 9, hence yielding 6 specific environments through which all adhesion assays were performed.

The number of micro beads as well as their fluorescence in solution was verified and quantified through flow cytometry (Supplementary information). This enabled adjustment to a standard micro bead concentration to approximately 5×10^5 micro beads/mL.

The surface energy properties of clean microbeads were obtained by contact angle measurements using MilliQ water, ethylene glycol, and diiodomethane sessile drops as described by Subramani and Hoek[8]. Briefly, microbead lawns were created on NF 270 membrane surfaces (Dow Filmtec,USA) through dead-end filtration at 15 bar(see supplementary information with SEM images showing full coverage of the NF270 surface of micro beads). The lawn was then allowed to dry overnight before contact angle experiments using a goniometer (OCA 20 Data physics instruments). The Lifshitz-van der Waals (γ^{LW}), electron-donor (γ^-) and electron-acceptor (γ^+) surface tension components of the micro bead surface (γ_S) were determined by measuring contact angles using the modified form of the extended Yong equation[16]:

$$\left(1 + \frac{\mathrm{Cos}\,\theta}{\mathrm{r}}\right)\gamma_{\mathrm{l}}^{\mathrm{TOT}} = 2\left(\sqrt{\gamma_{\mathrm{s}}^{\mathrm{LW}}\gamma_{\mathrm{l}}^{\mathrm{LW}}} + \sqrt{\gamma_{\mathrm{s}}^{+}\gamma_{\mathrm{l}}^{-}} + \sqrt{\gamma_{\mathrm{s}}^{-}\gamma_{\mathrm{l}}^{+}}\right) \qquad \text{(eq.1)}$$

Where r is defined as 'roughness area ratio', θ is the contact angle of the liquid on the solid surface and γ_l^{TOT} is the total surface energy. The substrates l and s represent the liquid and solid, accordingly [17].

The effect of ionic strength and pH on the microbead surface charge was assessed by measuring their electrophoretic mobility zetasizer (Malvern Zen 3600 Zetasizer, UK) under an electric field of 50V. The electrophoretic mobility of micro beads was performed in triplicate for each specific ionic and pH condition. Zeta-potential were obtained through the Helmholtz-Smoluchowski equation.

Substratum selection and characterization.

Two types of substrata were selected for this study to establish the effects of surface properties during adhesion. Glass slides (VWR) (50 by 13 mm) were chosen for their smooth flat surface and the NF90 (Dow Filmtech, USA) membrane was selected for its relatively hydrophobic surface properties. Prior to characterisation and adhesion experiments, the NF90membrane samples were rinsed and pre-soaked in MilliQ water and left submerged at 4°C overnight before being allowed to completely dry at room temperature.

Contact angle values and subsequent surface energy of both NF90 membranes and glass surfaces were obtained by using MilliQ water, ethylene glycol, and diiodomethane sessile drops as previously described by Heffernan et al. 2013 [18]. Contact angle measurements were made using a goniometer (OCA 20 Data physics instruments). Surface charge of glass and the NF90 membrane were determined through streaming potential measurements, after the surface samples were left to equilibrate in 0.1 M PBS solution overnight. Measurements were performed in triplicate using independent sample surfaces.

Direct microscopic observation setup.

Micro bead adhesion assays were performed as described by Semião et al. 2013, with slight modifications[19]. Membrane samples (2 x 3 cm) were immobilized onto glass slides using double sided tape (3M, Ireland), which were then fitted into individual flow cells (Model BST FC 81-AL, Biosurface Technologies Corporation, Bozeman, MT, USA) of channel dimensions 2.35 x 13 x 50 mm. Adhesion assays on glass were separately performed on fitted glass slides in the flow cell with the same channel dimensions. The dynamic adhesion experimental setup was composed of the flow cell devices, a peristaltic pump (Watson-Marlow UK 323E) and a container with the suspended micro beads in their respective PBS solutions, all connected with silicone tubing. The peristaltic pump was set at 100 rpm, corresponding to a volumetric flow rate of 92 mL/min.

The flow cells are small continuous-flow systems with a glass viewing port that allowed *in-situ* observation using an epi-fluorescence microscope (Olympus BX 51) and a 10x objective, corresponding to a field of view of 0.033 cm^2. After removing bubbles from the system, five random images were acquired around the central part of the membrane every five minutes for one hour, once the bead solution started flowing through the flow cell. Fluorescence emissions from the micro beads were captured using a U-MWB cube composed of a band pass excitation filter (BP460–490), a dichroic mirror (DM500), and a barrier long pass filter (BA 515). Images were obtained with a 1X CCD camera (Olympus, Japan), and recorded through Analysis® 3.2 imaging software. Adhesion assays were performed in triplicate using independent surface and micro bead solutions.

Adhesion computational analysis

Image analysis was performed using ImageJ (version 1.46r, National institute of health, USA) for determining the number of adhered micro beads as well as their radial distribution for each tested condition.

Radial distribution

The radial distribution functions for deposited beads were determined from an analysis of bead positions relative to other beads.The radial distribution function g(r) is defined as the relative number density(the ratio of counted beads to total beads in the screen) of the given deposited particle in a circular shellθ_i (r,dr), in which r represents the radius of the circle and dr is the thickness of the shell[13], as shown in Figure S6 in supplementary information.

The radial distribution function was determined once adhesion steady-state was reached and is defined by equations(2-4):

$$g(r) = \frac{\rho(r,dr)}{\rho_0} \quad \text{(eq.2)}$$

$$\rho(r,dr) = \frac{\sum_{i=1}^{N'_{tot}} N_i(r,dr)}{N'_{tot} \cdot A_{pix,\theta_i\,(r,dr)}} \quad \text{(eq.3)}$$

$$\rho_0 = \frac{N'_{tot}}{A_{pix,tot}} \quad \text{(eq.4)}$$

Where $N_i(r,dr)$ is the number of particles confined in the circle region θ_i (r,dr), N'_{tot} is the total number of particles in the image, $A_{pix,\theta_i\,(r,dr)}$ the pixel numbers in the circular shell θ_i (r,dr) and $A_{pix,tot}$ represents the total pixel numbers of the area of image. The radial distribution function correlates the number of particles and the number of pixels by converting the pixel number density into particle number density.

A previously deposited particle may prevent the subsequent particles from adhering on to nearby regions, which results in the kinetics levelling off at the later stage of adhesion test. The screen distance, which is a characteristic distance of the blocking effect, can be determined as the point of intersection of function g(r) with g(r)=1(Supplementary information)[13].

With equations (2-4), the screen distance of deposited particles can be determined. This will be used to calculate the desorption rate and to quantify the blocking effect in the adsorption-desorption kinetic model.

Adsorption-desorption kinetics

After three hours adhesion test, the number of adhered micro beads per unit area n(t) on the substratum will reach a plateau value, n_∞. The presence of deposited beads on the surface can prevent the adhesion of subsequent beads by" blocking " their deposition. As a result the adhesion rate decreases because of the 'blocked areas', A_1, the area blocked by one bead only[9].

$$J_{ads}(t) = J_0(1 - A_1 \cdot n(t)) \quad \text{(eq.5)}$$

$$A_1 = \pi R^2 \quad \text{(eq.6)}$$

Where J_{ads} is the adhesion rate of micro beads towards the surface of membrane (numbers cm^{-2} s^{-1}), J_0 is the initial adhesion rate of beads (numbers cm^{-2} s^{-1}) and R is the screen distance determined by radial distribution function.

At the same time, the desorption rate can be described as

$$J_{des}(t) = \beta \cdot n(t) \quad \text{(eq.7)}$$

Where β is the desorption rate constant in $s^{-1}cm^{-2}$. In Equation 6 desorption is assumed to be independent of time with the assumption that the final strength between bead and substratum surface remains constant upon its initial contact [20].

From Equations 6 and 7, the overall deposition rate of micro beads can be calculated as

$$J(t) = J_{ads}(t) - J_{des}(t) \quad \text{(eq.8)}$$

Integrating $J(t)$ over time t will give out the total number of beads adhered onto the substrate:

$$n(t) = \int_0^t J(t)dt = n_\infty(1 - e^{-(J_0 \cdot A_1 + \beta) \cdot t}) \quad \text{(eq.9)}$$

The deposition rate is assumed to level off eventually, and the initial adhesion rate can be easily deducted when adhesion assays reach steady state, i.e. Equation 8 equals zero, which is

$$J_0 = n_\infty \cdot (J_0 \cdot A_1 + \beta) \quad \text{(eq.10)}$$

To simplify computations, $J_0 \cdot A_1 + \beta$ was defined as a variable τ, in units of s^{-1}. A nonlinear regression algorithm was implemented to compute the two parameters, n_∞ and τ, from fitting of the counted number of beads to the theoretical model values given by Equation 9. The Lsqcurvefit function in MATLAB® was used to perform nonlinear regression fitting. With Lsqcurvefit inverting the variance/co-variance matrix Jacobian, reasonable *t*-distribution information can be combined to calculate the 95% confidence intervals of the two parameters mentioned in Equation 9.

The initial flux j_0 can be obtained from Equation 9 and desorption rate β can be further derived from τ by calculated the blocking area A_1. The radial distribution function was used to analyse all acquired images in this study.

Surface energy calculation based on XDLVO theory

The surface energies of polystyrene beads, glass and NF90 were evaluated using the Extended Derjaguin-Landau-Verwey-Overbeek (XDLVO) method. It consists of the attractive Lifshitz-van der Waals (LW) ,repulsive double layer (EL) and Lewis acid-base(AB) interactions.

$$U_{mlc}^{XDLVO} = U_{mlc}^{LW} + U_{mlc}^{EL} + U_{mlc}^{AB} \quad \text{(eq.11)}$$

From Equation 1, the non-polar LW γ^{LW} and polar AB components can be calculated. The Lewis-acid component γ^{AB} , which represents the polar surface tension, consists of two terms γ^+ and γ^-.

$$\gamma^{AB} = 2\sqrt{\gamma^+\gamma^-} \quad \text{(eq.12)}$$

The functionalities of Electron-acceptor (Lewis acid γ^+) and electon-donor (Lewis base γ^-) are estimated in the form of surface tensions. The total surface energy γ^{TOT} is the sum of the two surface tensions γ^{AB} andγ^{LW}.

Considering the surface tension of beads, substrate surfaces (i.e. membrane and glass) and the solution, the free energy between the bead and the substrates (ΔG^{LW} and ΔG^{AB}) can be evaluated.

$$\Delta G_{mlc}^{LW} = 2(\sqrt{\gamma_l^{LW}} - \sqrt{\gamma_m^{LW}})(\sqrt{\gamma_c^{LW}} - \sqrt{\gamma_l^{LW}}) \quad \text{(eq.13)}$$

$$\Delta G_{mlc}^{LW} = 2\sqrt{\gamma_l^+}\,(\sqrt{\gamma_m^-} + \sqrt{\gamma_c^-} - \sqrt{\gamma_l^-}) + 2\sqrt{\gamma_l^-}\,(\sqrt{\gamma_m^+} + \sqrt{\gamma_c^+} - \sqrt{\gamma_l^+}) - 2(\sqrt{\gamma_m^+\gamma_c^-} + \sqrt{\gamma_m^-\gamma_c^+}) \quad \text{(eq.14)}$$

Where the subscript l,m and c represent liquid, membrane and colloid respectively. The free energy of adhesion ΔG^{AD} per unit area is the sum of the two components and shows the interaction energy per unit area between two different surfaces, i.e. the surfaces between NF90/glass and beads.

The Gco is the interaction energy of solid surfaces immersed in water, and represents the hydrophobic/hydropholic nature of the material. GAB is the Gibbs energy of Acid-base interaction, and it is a component of GAD, the energy of adhesion[8].

The free energy of cohesion, ΔG^{CO} is the interaction energy per unit area of two surfaces of the same material are immersed in water and brought into contact. These values provide the quantative measurements of hydrophobicity/hydropholicity.

$$\Delta G_{mlm}^{LW} = -2(\sqrt{\gamma_l^{LW}} - \sqrt{\gamma_m^{LW}})^2 \quad \text{(eq.15)}$$

$$\Delta G_{mlm}^{LW} = 2\sqrt{\gamma_l^+}\,(2\sqrt{\gamma_m^-} - \sqrt{\gamma_l^-}) + 2\sqrt{\gamma_l^-}\,(2\sqrt{\gamma_m^+} - \sqrt{\gamma_l^+}) - 4\sqrt{\gamma_m^+\gamma_m^-} \quad \text{(eq.16)}$$

According to Brant and Childress [16], the LW interaction energy between a colloid and the membrane surface in liquid can be expressed by:

$$U_{mlc}^{LW} = 2\pi\,\Delta G_{y_o}^{LW}\,\frac{a_c}{h}\,y_0^2 \quad \text{(eq.17)}$$

where a_c represents the radius of the colloid, y is the separation distance between the colloid and the membrane; and y_0, with a value of 0.158 nm, is regarded as the distance between the van der Waals boundaries of non-covalently interacting molecules[17] .

The AB interaction energy decayed exponentially as the function of separation distance between two finite surfaces [16]:

$$\Delta G_y^{AB} = \Delta G_{y_0}^{AB} \exp[\frac{y_0 - y}{\lambda}] \quad \text{(eq.18)}$$

where λ is assigned a value of 0.6 nm, representing the characteristic decay length of AB interactions in water[16]. The AB interaction energy between the colloid and a membrane is:

$$U_{mlc}^{AB} = 2\pi a_c \lambda \, \Delta G_{y_0}^{AB} \exp[\frac{y_0 - y}{\lambda}] \quad \text{(eq.19)}$$

The EL interaction energy between a colloid and a membrane surface is the function of separation distance:

$$U_{mlc}^{EL} = \pi \varepsilon a_c \left(2\zeta_m \zeta_c \ln\left(\frac{1+e^{-\kappa h}}{1-e^{-\kappa h}}\right) + (\zeta_m^2 + \zeta_c^2) \ln\left(1 - e^{-2\kappa h}\right)\right) \quad \text{(eq.20)}$$

Where ε is the dielectric permittivity of water; ζ_m and ζ_c are the zeta potential of membrane and colloid, respectively; κ is the inverse Debye screening distance.

From Equations 17, 19 and 20, the total interaction energy between a colloid and membrane surface were calculated.

Surface coverage predictions with permeate flux

The parameters calculated from the kinetic model (desorption rate β, blocking area A_1) and the XDLVO interaction curve (using surface property and zeta potential values of micro beads) can be utilized to predict the surface coverage with permeate flux.

A permeate velocity of 1 μm/s is equivalent to 3.6 L/(hr m^2). The XDLVO migration velocity, v_{XDLVO} acts to attract micro bead to the membrane surface.

$$v_{XDLVO} \approx \frac{F_{XDLVO}}{f_{G0}} = \frac{F_{XDLVO}}{4.9\pi\mu {R_m}^{1/2} a^{3/2}} \quad \text{(eq.21)}$$

where f_{G0} is Goren's interfacial hydrodynamic correlation factor[21]. It consist of viscosity of the fluid μ, membrane hydraulic resistance R_m and the bead radius a.

In the solution chemistry of 0.1M NaCl, the migration velocities for model foulants approaching BW 30, NF90and ESNA1-FL2 are about 0.031, 0.233 and 0.239 μm/s, respectively. At pressure 3.1 bar, the permeate velocity for NF90is 0.62 μm/s so that the theoretical deposition velocity, v_{dep}, in this case is 0.853 μm/s. The initial adhesion rate can be calculated:

$$v_{dep} = \frac{J_0}{C_0} \qquad \text{(eq.22)}$$

where C_0 is the number concentration of micro beads in the feed solution[8].

From the radial distribution function analysis, the blocking area of bead onto NF90changes little with solution pH. It can be assumed that with the low permeate flux; the blocking area remains the same as that in flow cell. However, the desorption rate may decrease with the increasing permeate velocity, and in this case, a correction factor $\frac{v_{XDLVO}}{v_{dep}}$ was added to represent the effect of permeate velocity on the desorption rate.

$$\beta=\beta_0 \frac{v_{XDLVO}}{v_{dep}} \qquad \text{(eq.23)}$$

where β_0 is the desorption rate without permeate flux.

With these kinetic parameters calculated, the number of beads adhered onto the membrane at 30 minutes n(t) can be estimated from Equation 9. Assuming the projection area of a bead is πa^2, the surface coverage then can be easily solved.

RESULTS AND DISCUSSION

1. The surface physicochemical properties.

The characterisation of both microbeads and solid surfaces in terms of their physicochemical properties (Table 1) is an important preliminary step for investigating the experimental and

theoretical aspects of bead-surface interactions during this study. The surface energy data demonstrate that the two solid substrates have high electron donor components (γ^-) and relatively low electron acceptor component (γ^+). This is consistent with previous studies [8, 10, 16].Similarly, the electron donor component of micro beads was found to be a 100 times larger than the electron acceptor component. This implies that short-range acid-base interactions between micro beads and substrates are mainly repulsive because the electron donor components are predominantly high in NF90 and glass.

Using the physicochemical properties of micro-beads and solid surfaces, it was possible to work out the interfacial Gibbs energies between the bead and the substrates (Table 2). The Gibbs energy of adhesion ΔG^{AD} between micro bead and NF90 was found to be about 35% smaller than that of glass, which suggests that beads could encounter less repulsion when approaching NF90 compared to glass surfaces.

The energy of cohesion, ΔG^{CO}, defines the interaction energy when solid surface are immersed in the water[17]. The ΔG^{CO} of glass is double than that of NF90 membranes, due its higher electron donor component (γ^-), which also is an indication of the hydrophilic nature of glass Given these properties, it can be expected that glass surfaces may attract less micro-beads because of its high energy of cohesion.

Furthermore, it is possible to work out the bead-surface interaction energies using the equations 17-20 describing the attraction and repulsion state of a given bead as it approaches a given inert surface (Figure 1). At a given surface, a bead will first be attracted to the surface (i.e negative interaction energy), before encountering repulsive forces once in proximity to the surface. The existence of an interaction energy minimum is an indication of the likelihood of bead adhesion onto the NF90 and glass surfaces. Using the data obtained in Table 1 and 2, the secondary minimum for both glass- and NF90- type surfaces was calculated to be larger at high ionic strength, with interaction energy values of -38.05kT and -59.9 kT for glass and NF90 respectively. At lower ionic strengths however surface

interactions were calculated to be lower with values ranging from -12 kT to -18.2 kT for glass, and -15.08 kT to -24.10 kT for NF90 membranes. This is not unexpected since high salt concentrations compress surface electron double layers, resulting in lower electrostatic repulsive forces, hence favoring attraction.

Moreover, it also leads to the fact that the minimum energy varies little for the different pH studied at high ionic strength conditions (i.e. 0.1 M). At low ionic strength conditions (i.e. 0.01 M), the magnitude of secondary minimum at pH 9 on glass and NF90 were 27% and 37% lower than at pH 5 environments. This was observed as a shift in the interaction energy curve (Figure 1) indicating that beads encounter repulsion earlier at pH 9 compared to pH 5 and pH 7 environments.

The energy minimum can be used to predict the fouling tendency. At high ionic strength, the electron double layer is severely compressed, indicating that electrostatic (EL) repulsive forces are largely weakened. Although pH is considered as the main factor affecting micro-bead- and the membrane surface charge [6], the compressed EL interaction lead to insignificant variances of pH vlaues between curves at higher ionic strength environments.

2. Bead adhesion kinetic model fitting

To assess the degree of bead-surface interactions, bead deposition experiments were performed at various experimental conditions. The obtained data were fitted in kinetic model of adhesion (Figure 2). It was clearly observed that high ionic strength conditions led to increased bead adhesion on both NF90 (Figure 2A) and glass surfaces (Figure 2B). This can be explained by reduced electrostatic repulsion forces, in which beads encounter less resistance when approaching solid surfaces. From the XDLVO curves, the energy minimum at high ionic strength ranged from -55.90 to -56.03 kT while those numbers at low ionic strength changed from -15.08 to -24.1 kT. The same trend was also observed for beads adhering onto glass.

Micro-beads were observed to generally adhere less on bare glass compared to NF90. This preferential adhesion can be attributed to the lower free energy of adhesion ΔG^{AD} of the membrane surface. At low ionic strength conditions, the depth of energy on NF 90 membranes at pH 5, 7 and 9 environments were of the values of -24.10,-21.78 and -15.08 kT respectively, while for glass surfaces this depth of energy was found lower with values of -16.6, -18.17 and -11.99 kT respectively.

Presenting total number of bead adhesion only provide limited information. A fuller understanding of bead adhesion can be achieved by investigating bead initial adhesion rate J_0 using equation 10 (Table 3) based on fitting parameters n_∞ and τ.

Following the two parameter fitting of n_∞ and τ, a T-test (p=0.05) was performed to examine the effects of ionic strength, pH values and free energy of adhesion on the two tested surfaces types. Firstly, at high ionic strength conditions, the initial bead adhesion rate was found to be larger compared to low ionic situations. Secondly, the beads tend to adhere faster on the NF90 surface compared to the glass surface. This is not unexpected since the free energy of adhesion of NF90 surfaces was 26.96 mJ/m^2, about 33% lower than that of glass. It has also been observed by Subramani and Hoek that membranes with lower surface energies had greater bacterial adhesion[8]. In addition, pH values did not affect the adhesion rate significantly. For glass at high ionic strength environments, similar rates of adhesion were observed at both pH 5 and pH 7 (p>0.05), while at pH 9 the adhesion rate was reduced. For NF90 membranes at low ionic strength conditions, no significant differences were observed in adhesion rates conduced at pH 5 or pH 9, while higher rates were observed at pH 7.

3. The radial distribution of micro beads based on ionic strength and pH environments

With the radial distribution function analysis, the screening distances between the particles under different conditions were calculated. This made it possible to separate desorption rate β from the

fitting variable τ. As summarized in table 5, the screening distances between the beads on glass are slightly larger than that of the NF90 membrane, which indicated that the bead adhesion is more effective on NF 90 than glass. The type of substrate material was previously shown to affect blocking effect, as demonstrated by Sjollema and Busscher, who demonstrated that PMMA (polymethylmethacrylate)had smaller blocking effect than FEP (fluorethylenepropylene) or mica[13].Moreover, the tested pH values in their study were not shown to have a significant effect on screening distance.

The desorption rate β was separated from variable τ by simply subtracting the term $J_0 \cdot A_1$. On glass, desorption rate decreased with increasing pH while no clear trends were observed on NF90 membranes. The complex interplay between desorption and adsorption rates occur at the latter equilibrium stage of the adhesion process.

4. Adhesion rate correlation with XDLVO energy curve

Assessing adhesion rate as the function of the maximum attractive force F_{XDLVO} (Figure 3) was performed to detect potential correlations between experimental data obtained thus far and the theoretical interactions. According to Meinders et al, the maximum attraction force pulling the beads in the energy minimum, $F_{XDLVO,}$ was calculated from the slope of the XDLVO energy curve against the separation distance[10]. This value was shown to vary from 1.5×10^{-12} to 1.6×10^{-11} N for glass surfaces, and 1.7×10^{-12} to 2.6×10^{-11} N for NF 90 membranes. The higher adhesion rate on the NF90 can thus also be explained by the presence of stronger attractive forces. Moreover, at high ionic strength conditions, pH did not seem to significantly affect attractive forces, while at low ionic strength environments, the attractive force was weakest at pH9.

5. Model predictions under permeate flux conditions

Thus far, the experimental data described the adhesion of beads onto NF 90 membranes at various environmental conditions under zero flux conditions. Permeate flux, is relevant in a real filtration context, since permeation drag has been shown to overwhelm the interfacial forces and dominate the initial adhesion[8]. This has also been shown in one recent study in which the surface coverage of *Pseudomonas fluorescens* onto various NF and RO membranes increased with increasing permeate flux conditions[22] .

Nevertheless, two essential questions need to be asked; i) do surface properties affect initial bacterial adhesion at low flux and , ii) at which point the permeate drag start to control the adhesion process?

In order to answer these questions, it is essential to characterize the physicochemical properties of the bacterial cells being studied. In an earlier study, Chen and Strevett have measured the surface properties of *P. fluorescens* at stationary state in the buffer solution (potassium phosphate monobasic–sodium hydroxide buffer)[23], which have been compared to the micro-beads used in this study (Table 6). Although the beads used in this study showed about 10% higher surface energies than *P. fluorescens*, it can be considered safe to predict *P. fluorescens* surface coverage under permeate flux conditions using the surface properties of micro beads (Figure 4 A,B and C).

From the model predictions, it was possible to investigate the initial adhesion on different membranes at low permeate flux conditions (up to 7.2 L m^{-2} hr^{-1}), as shown in Figure 4(D). With higher hydraulic membrane resistance R_m of 1.03×10^{16} m^{-1}, the bacteria migration velocity towards the surface of a BW 30 RO membrane was found to be significantly reduced, resulting to lower surface coverage. However, for some other membranes showing similar hydraulic resistance, the interaction force between the bacteria and the membrane surface was found to dominate the initial adhesion process. For membranes having stronger attractive forces, such as ESNA1-LF2, bacterial adhesion was initially favored at low permeate conditions. However, as the permeate velocity increases to about 2 µm/s (equivalent to permeate flux of 7.2L hr^{-1} m^{-2}), all predicted

adhesion curves converged, signifying that membrane surface property differences become irrelevant at a certain system dependent critical permeate flux, hence dominating the adhesion process. The surface coverage prediction of NF 90,BW 30 and ESNA1-FL2 with larger permeate flux values has been provided in the supplementary information. According to Subramani and Hoek, permeation drag overwhelms interfacial forces at permeate flux higher than 20 L hr^{-1} m^{-2} for NF90at ionic strength of 0.01 M[8]. The high ionic strength 0.1M compresses the double layer electronic repulsion and the permeate drag takes over the process at relatively small flux in this case[8]. It shows that the both the environmental and operation condition affect the initial adhesion in membrane process.

Conclusion:

In this study, a novel experimental method was implemented by maximizing the amount of acquired adhesion images, in order to assess the statistical quality of the experimental outcome. The real time adhesion data was interpreted by the kinetic model which consists of adsorption and desorption rate. Unlike the image subtraction techniques used by Meiders et al, the radial distribution function was utilized in the image analysis to study the blocking effects of the already adhered beads. Moreover, few papers have correlated the interaction energy between the bead and the nano-filtration membrane with the adsorption-desorption kinetic model. This combination of XDLVO theory with kinetic model allows a better understanding of the initial adhesion under permeate flux conditions.

Acknowledgements

This work was supported by the European Research Council (ERC), under grant number 278530 and also with the financial support of Science Foundation Ireland under Grant Number “SFI 11/RFP.1/ENM/3145. The authors thank Dr. Alfonso Blanco from Conway Institute, UCD for his

invaluable technical assistance. We thank Dr. Dermot Malone for his assistance in adsorption-desorption kinetic model fitting.

References

[1] H.C. Flemming, G. Schaule, T. Griebe, J. Schmitt, A. Tamachkiarowa, Biofouling—the Achilles heel of membrane processes, Desalination, 113 (1997) 215-225.
[2] H.-C. Flemming, Biofouling in water systems–cases, causes and countermeasures, Applied Microbiology and Biotechnology, 59 (2002) 629-640.
[3] G.G. Geesey, Biofouling and biocorrosion in industrial water systems, CRC Press, 1994.
[4] H. Ridgway, H. Flemming, Microbial adhesion and biofouling of reverse osmosis membranes, Reverse Osmosis Technology: Applications for High Purity Water Production, ed. by BS Pakekh and M. Dekker, (1988) 429-481.
[5] S. Bayoudh, A. Othmane, L. Mora, H. Ben Ouada, Assessing bacterial adhesion using DLVO and XDLVO theories and the jet impingement technique, Colloids and Surfaces B: Biointerfaces, 73 (2009) 1-9.
[6] O. Habimana, A.J.C. Semião, E. Casey, The role of cell-surface interactions in bacterial initial adhesion and consequent biofilm formation on nanofiltration/reverse osmosis membranes, Journal of Membrane Science, 454 (2014) 82-96.
[7] J. Li, H.J. Busscher, W. Norde, J. Sjollema, Analysis of the contribution of sedimentation to bacterial mass transport in a parallel plate flow chamber, Colloids and Surfaces B: Biointerfaces, 84 (2011) 76-81.
[8] A. Subramani, E.M.V. Hoek, Direct observation of initial microbial deposition onto reverse osmosis and nanofiltration membranes, Journal of Membrane Science, 319 (2008) 111-125.
[9] R. Bos, H.C. Mei, H.J. Busscher, Physico - chemistry of initial microbial adhesive interactions–its mechanisms and methods for study, FEMS microbiology reviews, 23 (1999) 179-230.
[10] J.M. Meinders, H.C. van der Mei, H.J. Busscher, Deposition Efficiency and Reversibility of Bacterial Adhesion under Flow, Journal of Colloid and Interface Science, 176 (1995) 329-341.
[11] A.I. Radu, J.S. Vrouwenvelder, M.C.M. van Loosdrecht, C. Picioreanu, Modeling the effect of biofilm formation on reverse osmosis performance: Flux, feed channel pressure drop and solute passage, Journal of Membrane Science, 365 (2010) 1-15.
[12] D.J. Miller, P.A. Araújo, P.B. Correia, M.M. Ramsey, J.C. Kruithof, M.C.M. van Loosdrecht, B.D. Freeman, D.R. Paul, M. Whiteley, J.S. Vrouwenvelder, Short-term adhesion and long-term biofouling testing of polydopamine and poly(ethylene glycol) surface modifications of membranes and feed spacers for biofouling control, Water Research, 46 (2012) 3737-3753.
[13] J. Sjollema, H.J. Busscher, Deposition of polystyrene particles in a parallel plate flow cell. 2. Pair distribution functions between deposited particles, Colloids and Surfaces, 47 (1990) 337-352.
[14] S.L. Walker, J.A. Redman, M. Elimelech, Influence of Growth Phase on Bacterial Deposition: Interaction Mechanisms in Packed-Bed Column and Radial Stagnation Point Flow Systems†, Environmental Science & Technology, 39 (2005) 6405-6411.
[15] S. Perni, E.C. Preedy, P. Prokopovich, Success and failure of colloidal approaches in adhesion of microorganisms to surfaces, Advances in Colloid and Interface Science, 206 (2014) 265-274.
[16] J.A. Brant, A.E. Childress, Assessing short-range membrane–colloid interactions using surface energetics, Journal of Membrane Science, 203 (2002) 257-273.
[17] C.J. van Oss, Hydrophobicity of biosurfaces — Origin, quantitative determination and interaction energies, Colloids and Surfaces B: Biointerfaces, 5 (1995) 91-110.
[18] R. Heffernan, A.J.C. Semião, P. Desmond, H. Cao, A. Safari, O. Habimana, E. Casey, Disinfection of a polyamide nanofiltration membrane using ethanol, Journal of Membrane Science, 448 (2013) 170-179.

[19] A.J.C. Semião, O. Habimana, H. Cao, R. Heffernan, A. Safari, E. Casey, The importance of laboratory water quality for studying initial bacterial adhesion during NF filtration processes, Water Research, 47 (2013) 2909-2920.
[20] T. Dabroś, T.G.M. Van De Ven, On the effects of blocking and particle detachment on coating kinetics, Journal of Colloid and Interface Science, 93 (1983) 576-579.
[21] S.L. Goren, The hydrodynamic force resisting the approach of a sphere to a plane permeable wall, Journal of Colloid and Interface Science, 69 (1979) 78-85.
[22] A.J.C. Semião, O. Habimana, E. Casey, Bacterial adhesion onto nanofiltration and reverse osmosis membranes: Effect of permeate flux, Water Research, 63 (2014) 296-305.
[23] G. Chen, K.A. Strevett, Microbial surface thermodynamics and interactions in aqueous media, Journal of Colloid and Interface Science, 261 (2003) 283-290.

Table 1 Calculated surface energies (mJ/m^2) of substrates and micro beads

	γ^{LW}	γ^{+}	γ^{-}	γ^{AB}	γ^{TOT}
Glass	36.569±3.324	0.238±0.237	58.459±5.697	7.460±0.363	44.029±3.344
NF 90	41.105±0.446	0.083±0.095	37.409±4.118	3.524±0.193	44.629±0.486
Micro beads	48.905±0.385	0.467±0.082	59.818±2.592	10.571±1.296	59.476±1.352

Table 2: Interfacial Gibbs energies between bead and substrates, in mJ/m^2

	ΔG^{LW}	ΔG^{AB}	ΔG^{CO}	ΔG^{AD}
Glass	-6.486	47.162	43.514	40.676
NF 90	-8.186	34.876	14.166	26.69

Table 3. Kinetic fitting results of n_∞,parameter τ and initial bead adhesion rate J_0 for glass and NF90

Glass	$n_\infty(cm^{-2})$	$\tau(10^{-4}s^{-1})$	$Jo(s^{-1}\,cm^{-2})$
0.01M pH5	3802±372	5.29±1.03	2.01±0.43
0.01M pH7	4652±784	3.09±0.80	1.43±0.44
0.01M pH9	9050±3638	1.76±0.90	1.59±1.03
0.1M pH5	9009±1720	4.51±1.57	4.07±1.61
0.1M pH7	9257±953	4.27±0.78	3.95±0.83
0.1M pH9	11870±1692	2.00±0.38	2.37±0.56
NF 90	$n_\infty(cm^{-2})$	$\tau(10^{-4}s^{-1})$	$Jo(s^{-1}\,cm^{-2})$
0.01M pH5	11099±4899	2.42±0.92	2.69±0.84
0.01M pH7	5662±200	8.05±0.74	4.56±0.45
0.01M pH9	6715±377	5.45±0.62	3.66±0.46
0.1M pH5	18349±1511	3.44±0.45	6.31±0.97
0.1M pH7	22170±3038	1.72±0.46	5.63±1.27
0.1M pH9	23109±4297	2.21±0.56	5.13±1.61

Table4. T-test of ionic strength, pH and different surface effects on initial adhesion rate

P=0.05	pH effects (Glass)	t value	pH effects (NF90)	t value	ionic strenth	t value	t test of surface energy	t value
2.048	pH5 vs pH7(0.01M)	1.83	pH5 vs pH7(0.01M)	3.23	0.01M & 0.1M (Ph5,glass)	6.6	Glass& NF 90 (pH5 0.01M)	2.06
2.048	pH5 vs pH9(0.01M)	0.73	pH5 vs pH9(0.01M)	1.36	0.01M & 0.1M (pH7,glass)	14.41	Glass& NF 90 (pH7 0.01M)	9.74
2.048	pH7 vs pH9(0.01M)	0.28	pH7 vs pH9(0.01M)	2.73	0.01M & 0.1M (pH9,glass)	3.56	Glass& NF 90 (pH9 0.01M)	3.56
2.048	pH5 vs pH7(0.1M)	0.13	pH5 vs pH7(0.1M)	0.83	0.01M & 0.1M (pH5,NF90)	13.84	Glass& NF 90 (pH5 0.1M)	2.33
2.048	pH5 vs pH9(0.1M)	1.95	pH5 vs pH9(0.1M)	1.23	0.01M & 0.1M (Ph7,NF 90)	4.26	Glass& NF 90 (pH7 0.1M)	2.17
2.048	pH7 vs pH9(0.1M)	3.09	pH7 vs pH9(0.1M)	0.48	0.01M & 0.1M (Ph9, NF 90)	4.7	Glass& NF 90 (pH9 0.1M)	3.17

Table 5. Screening distance of beads and desorption rate β

	Glass			NF 90		
	$\beta(10^{-4}\ s^{-1})$	Screening distance (μm)	Blocking area(10^{-6} cm2)	$\beta(10^{-4}\ s^{-1})$	Screening distance (μm)	Blocking area(10^{-6} cm2)
0.01M pH5	5.18	13.04	5.34	2.36	8.69	2.37
0.01M pH7	3.02	13.04	5.34	7.61	17.38	9.48
0.01M pH9	1.76	26.03	21.28	5.36	8.69	2.37
0.1M pH5	4.51	13.04	5.34	3.29	8.69	2.37
0.1M pH7	4.27	17.38	9.49	2.32	8.69	2.37
0.1M pH9	1.96	13.04	5.34	2.09	8.69	2.37

Table6. Surface properties of micro beads and P*seudomonas fluorescens* at stationary state

	γ^{LW}	γ^{+}	γ^{-}	γ^{AB}	γ^{TOT}
Pseudomonas fluorescens[*]	36.5	1.29	56.8	17.12	53.62
Micro beads	48.9±0.385	0.47±0.08	59.8±2.6	10.6±1.3	59.5±1.4

*values from Chen and Strevett [23]

Figure Legends

Figure 1 The interaction energy between a bead and the solid surface (A: NF90, B: Glass; at different pH and ionic strength environments)

Figure2 The bead adhesion on two solid surfaces (scattered points with error bars are the experiment data, and the solid lines are the fitting curve, ●,▼,■ for pH5, 7 and 9 at ionic strength of 0.1M;○, ▽,□ for pH5, 7 and 9 at ionic strength of 0.01M)

Figure 3 The initial adhesion flux, j_0, of polystyrene beads depositing to glass (A) and NF90(B) from PBS solutions with different ionic strengths and pH values as a function of maximum attraction force F_{XDLVO}

Figure 4. The surface coverage of NF90, BW30 and ESNA1-LF2(scattered dots: experimental data and lines: predicted results)

Figure 1

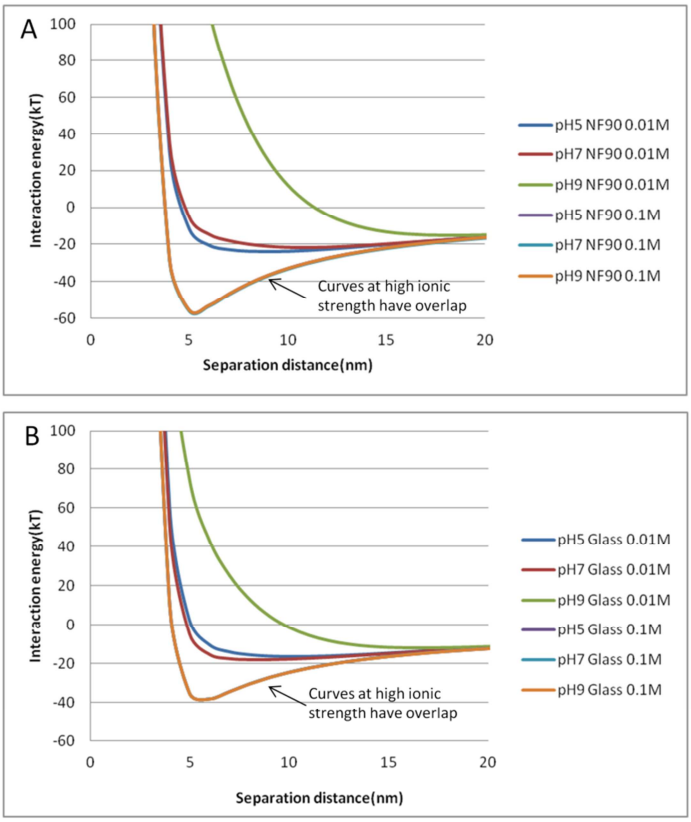
A
100
80
60
40
20
0
-20
-40
-60
Interaction energy(kT)
0
5
10
15
20
Separation distance(nm)
Curves at high ionic strength have overlap
pH5 NF90 0.01M
pH7 NF90 0.01M
pH9 NF90 0.01M
pH5 NF90 0.1M
pH7 NF90 0.1M
pH9 NF90 0.1M
B
100
80
60
40
20
0
-20
-40
-60
Interaction energy(kT)
0
5
10
15
20
Separation distance(nm)
Curves at high ionic strength have overlap
pH5 Glass 0.01M
pH7 Glass 0.01M
pH9 Glass 0.01M
pH5 Glass 0.1M
pH7 Glass 0.1M
pH9 Glass 0.1M

Figure 2

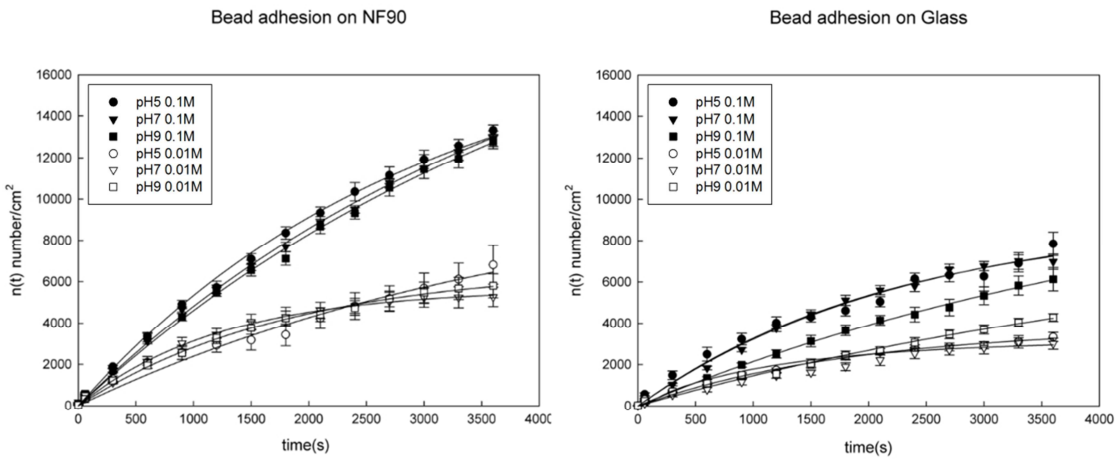
Bead adhesion on NF90
Bead adhesion on Glass
pH5 0.1M
pH7 0.1M
pH9 0.1M
pH5 0.01M
pH7 0.01M
pH9 0.01M
n(t) number/cm2
time(s)
0
2000
4000
6000
8000
10000
12000
14000
16000
500
1000
1500
2000
2500
3000
3500
4000

Figure 3

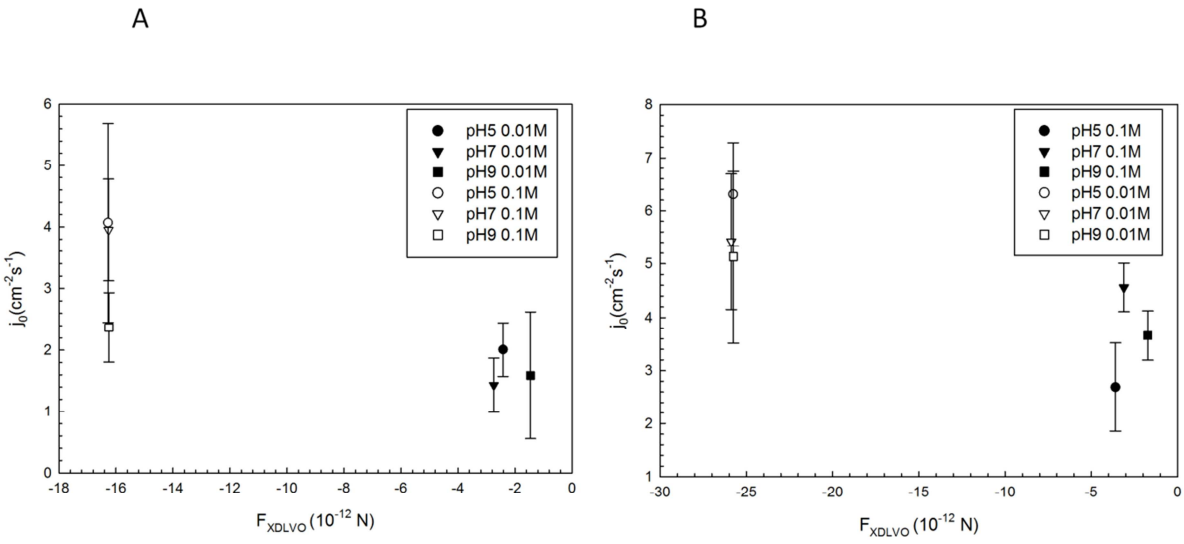
A
B
pH5 0.01M
pH7 0.01M
pH9 0.01M
pH5 0.1M
pH7 0.1M
pH9 0.1M
$j_0(cm^{-2}s^{-1})$
F_{XDLVO} (10^{-12} N)

Figure 4

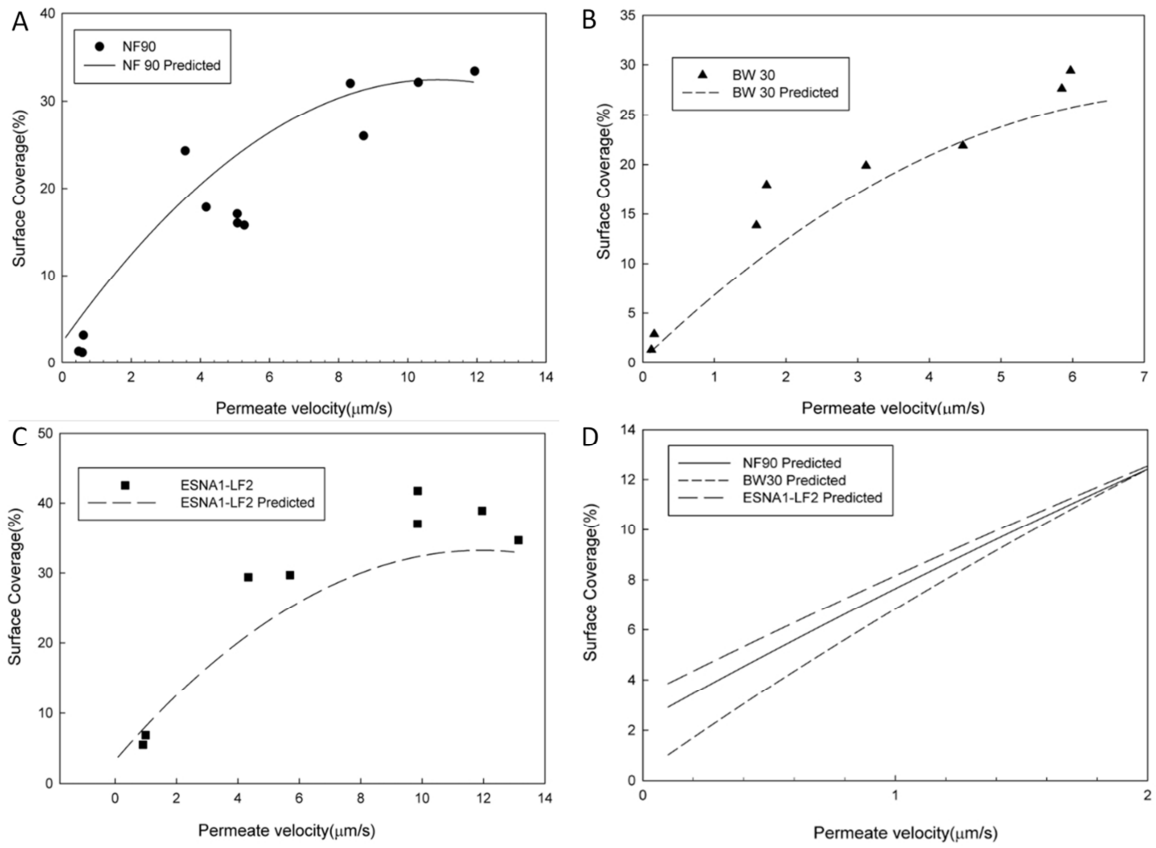
A
NF90
NF 90 Predicted
Surface Coverage(%)
Permeate velocity(μm/s)
B
BW 30
BW 30 Predicted
Surface Coverage(%)
Permeate velocity(μm/s)
C
ESNA1-LF2
ESNA1-LF2 Predicted
Surface Coverage(%)
Permeate velocity(μm/s)
D
NF90 Predicted
BW30 Predicted
ESNA1-LF2 Predicted
Surface Coverage(%)
Permeate velocity(μm/s)